

Characterization of Nuclear and Magnetic Structures of Wolframite-Type MgReO_4 and ZnReO_4

U. Miniotaitte ^{1*}, O.K Forslund^{2,3} E. Nocerino ^{4,5} Y. Ge ¹, F. Elson ¹, M. Sannemo ⁶,
H. Sakurai ⁷, J. Sugiyama ⁸, H. Luetkens ⁵, T. Ishigaki ⁹, T. Hawaii ⁹, R. Palm ¹⁰,
C. Wang ⁵, Y. Sassa ¹, D. W. Tam ¹, M. Månsson ^{1**}

1 Department of Applied Physics, KTH Royal Institute of Technology, SE-106 91
Stockholm, Sweden

2 Physik-Institut, Universität Zürich, Zürich, Switzerland

3 Department of Physics and Astronomy, Uppsala University, Uppsala, Sweden

4 Department of Chemistry, Stockholm University, Stockholm, Sweden

5 PSI Center for Neutron and Muon Sciences CNM, Villigen PSI, Switzerland

6 Department of Materials and Environmental Chemistry, Stockholm University,
Stockholm, Sweden

7 National Institute for Materials Science (NIMS), Namiki Tsukuba Ibaraki, Japan

8 Neutron Science and Technology Center, Comprehensive Research Organization for
Science and Society (CROSS), Tokai, Japan

9 Neutron Industrial Application Promotion Center, Comprehensive Research
Organization for Science and Society (CROSS), Tokai, Japan

10 Institute of Chemistry, University of Tartu, Tartu, Estonia

* ugnem@kth.se ** condmat@kth.se

March 26, 2025

Abstract

We utilized high-pressure methods to synthesize the oxides AReO_4 ($\text{A} = \text{Zn}, \text{Mg}$) and characterized their crystal structures as monoclinic wolframite-type. By combining muon spin spectroscopy ($\mu^+\text{SR}$) with DFT calculations for muon stopping sites, we identify two possible magnetic spin structures for both compounds: Γ_3 with the propagation vector $\mathbf{k} = (0, 1/2, 0)$ and Γ_4 with $\mathbf{k} = (0, 0, 0)$. In both cases, the magnetic moments are canted from the principal axes within the ac -plane. The ordered moment of the proposed structures is $0.29(5)\mu_B$ for Γ_3 and $0.25(8)\mu_B$ for Γ_4 . The low moment is consistent with the absence of a magnetic contribution to the neutron powder diffraction (NPD) spectra. Bond valence sum (BVS) analysis supports the oxidation state of Re being Re^{6+} in the compounds and we suggest that a combination of t_{2g} orbital splitting due to spin-orbit coupling (SOC) and d - p orbital hybridization is responsible for the strongly suppressed ordered magnetic moment.

Contents

1	Introduction	2
2	Experimental Methods	3
3	Results	4

3.1	Neutron Powder Diffraction	4
3.2	Muon Spin Spectroscopy	5
3.2.1	MgReO ₄	7
3.2.2	ZnReO ₄	9
3.3	Muon site and field calculations	9
3.4	Bond Valence Sum	10
4	Discussion	15
5	Conclusions	16
A	AC Magnetic Susceptibility	17
B	XRD analysis	18
C	Zero Field	19
D	Longitudinal Field	19
E	Transverse Field	21
F	Canting in MgReO₄	23
	References	25

1 Introduction

Transition metal oxides play a fundamental role in condensed matter physics due to their diverse and unique states, such as high-temperature superconductivity [1, 2], exotic magnetic phases [3–5], multiferroics [6, 7] and metal-insulator transitions [8, 9]. This family also show their importance in applications, e.g., energy storage (rechargeable batteries) [10–12] and catalysis [13, 14]. Their wide variety of properties are attributed to variations in oxygen bonding and the nature of the unfilled d electron shells [15].

Rhenium, the last transition metal to be discovered in 1925 [16], has attracted interest for its broad range of oxidation states (-3 to +7) [17]. At the higher end of oxidation, we find the rhenium oxides and halides. Rhenium oxides often stabilize in the perrhenate structure in which oxygen atoms form a tetrahedral coordination around the Re atoms [18–20]. Some well-known AReO₄ perrhenates, where A is a metallic cation and Re is in the +7 oxidation state, include AgReO₄ [21] and KReO₄ [22], both utilized in electrochemical applications. However, there are only a few reports of such compounds with Re in a lower oxidation state [23–26].

In the 1970s, Sleight *et al.* synthesized a series of AReO₄ oxides which were found to have rutile ($A = \text{Al, Fe, Ga}$) and wolframite-type ($A = \text{Mg, Mn, Zn}$) structures. The goal was to stabilize rhenium in lower oxidation states [23] and to combine localized $3d$ electrons with delocalized $5d$ electrons, potentially leading to novel electronic and magnetic properties. Based on bond length estimates from lattice parameters, most rutile compounds were assigned a Re⁵⁺ oxidation state, while the wolframite-type oxides were assigned Re⁶⁺ [23]. Notably, Re⁶⁺ compounds exhibit intriguing magnetic properties,

including weak persistent ferromagnetism (FM) above room temperature [27–29] and pronounced magnetic anisotropy [30, 31]. The wolframite structure, consists of edge-sharing, distorted octahedral coordination of oxygen around Re atoms. The origin of octahedral distortions in rhenium oxides has been attributed to Jahn-Teller (JT) effects [32], Re-Re bonding [33], or variations in ionic radii [34].

Among these compounds, Bramnik *et al.* [35] have characterized the wolframite structure of MnReO_4 and, through magnetic susceptibility measurements, identified an antiferromagnetic (AFM) component with a Néel temperature, T_N , of 280 K, coexisting with weak FM below the Curie temperature of 225 K. Mn in MnReO_4 possesses unpaired electrons, leading to strong magnetic moments which obscure the contribution from Re^{6+} . In contrast, neither Mg in MgReO_4 nor Zn in ZnReO_4 has unpaired electrons, meaning that any magnetism in these compounds originates solely from Re^{6+} , making them ideal candidates for studying its intrinsic magnetism.

In this study, we investigate the magnetic properties of the wolframite-type rhenium oxides AReO_4 ($A = \text{Mg}, \text{Zn}$). To characterize their structure, we conduct neutron powder diffraction (NPD). The diffraction patterns show no visible magnetic contributions for either sample at 7 K, despite clear magnetic transitions observed in both AC magnetic susceptibility (ACMS) and muon spin spectroscopy ($\mu^+\text{SR}$), indicating a weak magnetic moment.

Our preliminary analysis of MgReO_4 using $\mu^+\text{SR}$ identified AFM ordering below $T_N = 83$ K [36]. At base temperature ($T = 2$ K), two muon precession frequencies were observed, originating from two distinct muon stopping sites. However, above $T = 60$ K, only one precession frequency is present in the data. This was initially speculated to be a result from spin canting, causing both muon sites to experience the same magnetic moment.

Here, we provide a more detailed analysis of the MgReO_4 $\mu^+\text{SR}$ data [36] and extend the study to ZnReO_4 . We revisit the MgReO_4 $\mu^+\text{SR}$ data reported in [36] with the advantage of a refined crystal structure from complementary NPD data, gaining additional insights into the system’s magnetic properties. Using a combination of DFT, $\mu^+\text{SR}$ and NPD, we identify two possible magnetic structures for both compounds consistent with zero field (ZF) $\mu^+\text{SR}$ data. By examining the magnetic structure under canting conditions, we rule out spin canting as the cause of the reduction in observed muon precession frequencies. Bond valence sum (BVS) analysis supports the Re^{6+} oxidation state, ruling out wrongful oxidation state as the cause of the low observed ordered moment. Instead, our results suggest that strong spin-orbit coupling (SOC) in the $5d^1$ system splits the t_{2g} orbitals, with the lowest energy level being a non-magnetic quadruplet state, causing the suppressed magnetic moment.

2 Experimental Methods

High-quality powder samples of ZnReO_4 and MgReO_4 were synthesized at the National Institute for Materials Science (NIMS), Ibaraki, Japan, using a high-pressure synthesis technique. The material was subjected to a pressure of 6 GPa for one hour, at a temperature of 1300 °C. As the samples are sensitive to humidity, in particular ZnReO_4 , all sample preparations were conducted in an Argon glove box.

To ensure sample quality, due to the high humidity sensitivity, ZnReO_4 was checked using ACMS (Appendix A). ACMS measurements were conducted using the Quantum Design PPMS DynaCool. The sample was compressed inside a capsule and sealed with kapton tape.

NPD was used to characterize the structures. The NPD patterns were collected at high-resolution time-of-flight (TOF) diffractometer iMATERIA at J-PARC [37], Ibaraki, Japan. Approximately 0.5 g of each sample was sealed in a cylindrical vanadium can (diameter 5 mm) using aluminium screws and indium wire. For structural refinement, the high-Q detector banks; back scatter (BS) with resolution $\Delta d/d = 0.15\%$ and 90° SE detector bank with resolution $\Delta d/d = 0.45\%$, were used. The diffraction spectra were refined together using `FULLPROF SUITE` [38]. We also attempted to characterize the structures using X-ray diffraction (XRD), but due to high X-ray absorption of rhenium and reactions with grease, this was unsuccessful (see Appendix B).

The General Purpose surface muon beamline (GPS) at the Paul Scherrer Institute (PSI) in Villigen, Switzerland, was used to conduct the μ^+ SR experiments. Approximately 200 mg each of ZnReO_4 and MgReO_4 was sealed with Kapton tape inside an aluminum mylar-tape envelope (thickness $\approx 50 \mu\text{m}$). The sample was then mounted on a low-background copper fork and inserted into a He-4 flow cryostat, allowing for a temperature range of $T = 2 \text{ K} - 300 \text{ K}$.

The μ^+ SR measurements were performed in different magnetic field configurations, defined by the field alignment relative to the initial muon spin polarization: zero field (ZF), transverse field (TF), and longitudinal field (LF). In ZF, no external field is applied. In TF, the field is perpendicular to the initial muon spin polarization, while in LF, it is applied parallel to the polarization.

ZF spectra were collected for ZnReO_4 between $T = 2 \text{ K}$ and 140 K , and for MgReO_4 between $T = 2 \text{ K}$ and 100 K . TF measurements were performed using a magnetic field of $B = 50 \text{ G}$, while LF spectra were measured with $B = 10 \text{ G}$ and $B = 20 \text{ G}$. The data was analyzed using the `musrfit` software [39].

The electrostatic landscapes were calculated using the pseudopotential-based plane-wave method as implemented in `QUANTUM ESPRESSO` [40]. Based on the obtained muon site candidates, the local magnetic fields were evaluated for different spin configurations using the package `muesr` in Python [41].

3 Results

3.1 Neutron Powder Diffraction

NPD was used to determine the crystal structure and atomic positions in MgReO_4 and ZnReO_4 . A comparison of the diffraction patterns collected above T_N and at 7 K shows no evidence of a structural transition or appearance of a magnetic contribution to the pattern in any of the detector banks [insets Fig. 1 (a)-(b)]. This may on a first glance contradict the proposition of the samples being magnetically ordered. However, as we shall show below (Sec. 3.3), the absence of a magnetic contribution is consistent with small ordered moments which can also explain our μ^+ SR results. Low magnetic moments have resulted in the absence of magnetic peaks in NPD in other Re^{6+} systems [42, 43].

The crystal structure refinement was performed using the patterns collected at 7 K to maximize the accuracy of the magnetic dipole field calculations (Sec. 3.3). The measured patterns [Fig. 1 (a)-b)] were refined to a monoclinic wolframite-type structure with the space group $\text{P}2/c$ (# 13) [44]. The refined lattice parameters [Tab. 1] are close to the values found by Sleigh *et al.* [23]. The structure [Fig. 1 (c)-(d)] contains edge-sharing distorted octahedral coordination of O surrounding the Re atoms. The octahedra form a zig-zag pattern along the c -axis and sandwiches the Mg/Zn atoms along the a -axis. In the distorted octahedra of both samples, the O-Re-O bond angles range from 76° to 101° ,

deviating from the ideal 90° . Additionally, the octahedra are compressed along the a -axis and elongated along the c -axis. The Re center is also displaced along the b -axis, leading to varying Re-Re distances along this direction. These distortions are very similar in both compounds and resemble MnReO_4 , which has bond angle variation of 81.9° to 101.9° [35].

MgReO_4	
Crystal structure	monoclinic P2/c
a, b, c (\AA)	4.67703, 5.57462, 5.01010
β ($^\circ$)	91.9017
V (\AA^3)	130.5547
Mg (x, y, z)	(0.5, 0.678, 0.25)
Re (x, y, z)	(0, 0.169, 0.25)
O1 (x, y, z)	(0.217, 0.111, 0.943)
O2 (x, y, z)	(-0.258, 0.627, 0.608)
Refinement	
χ^2	0.3543
ZnReO_4	
Crystal structure	monoclinic P2/c
a, b, c (\AA)	4.68845, 5.60300, 5.02260
β ($^\circ$)	91.2713
V (\AA^3)	132.2557
Zn (x, y, z)	(0.5, 0.686, 0.25)
Re (x, y, z)	(0, 0.166, 0.25)
O1 (x, y, z)	(0.214, 0.115, 0.947)
O2 (x, y, z)	(-0.250, 0.636, 0.613)
Refinement	
χ^2	0.1231

Table 1: Crystal structure parameters of ZnReO_4 and MgReO_4 from refinement of neutron powder diffraction data.

Both samples exhibit impurity peaks around $Q = 1.8 - 2 \text{ \AA}$, as well as dispersed peaks at higher Q in the spectra. The impurities could not be refined to any known compound containing O, Re, and/or Mg/Zn, and the regions containing these peaks were therefore excluded from the refinement. Since the impurity peaks remain visible above T_N , they do not seem to be of magnetic origin. They might represent a mix of multiple compounds formed during the high-pressure synthesis process. This impurity could also be accounted for as a paramagnetic, exponentially decaying signal in the μ^+ SR data (Sec. 3.2).

3.2 Muon Spin Spectroscopy

To gain information about the magnetic structures, we conduct a μ^+ SR study on both MgReO_4 and ZnReO_4 as a function of temperature. The ZF μ^+ SR time spectra of ZnReO_4 and MgReO_4 is presented in Fig. 2. The ZF time spectra at low temperatures reveals multiple oscillations in both samples. The presence of oscillations indicates magnetic ordering and multiple oscillations suggests multiple muon stopping sites inside the crystal structure. In a powder, two thirds of the internal magnetic field components are expected to be perpendicular to the initial muon spin polarization (causing oscillations), whereas

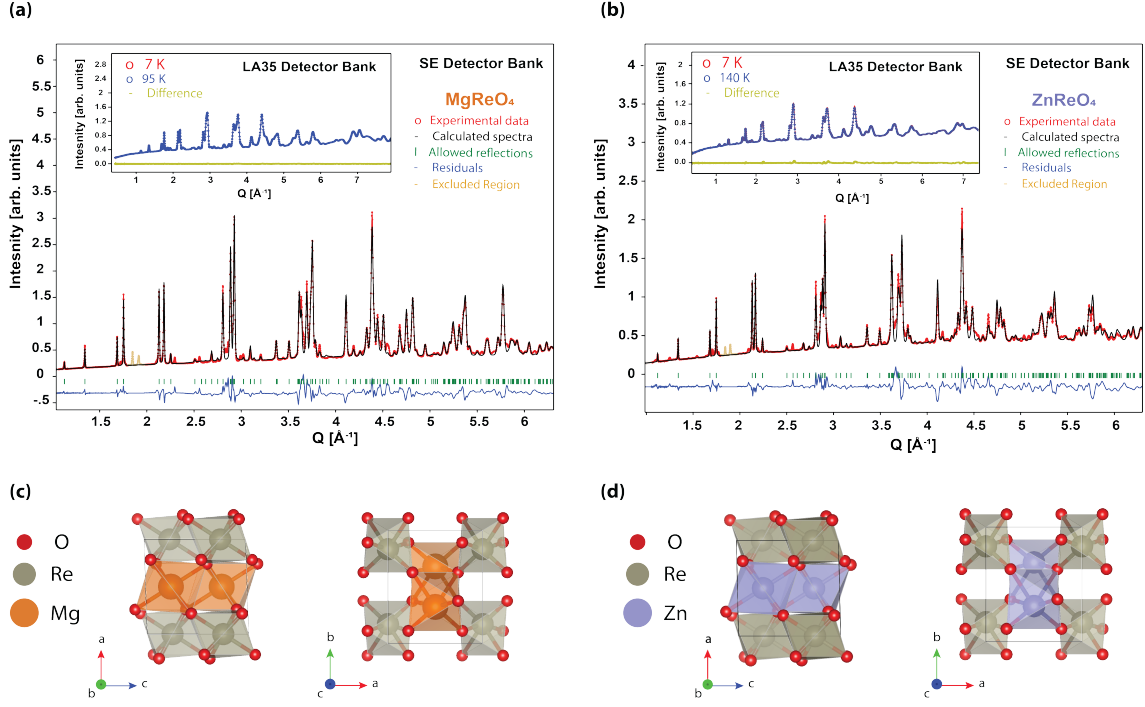


Figure 1: Measured neutron powder diffraction (NPD) patterns, refined spectra, allowed reflections, and residuals for data collected at 7 K from the SE detector bank for (a) MgReO₄ and (b) ZnReO₄. Regions excluded due to impurities are colored in orange. The insets show the differences between patterns obtained from the low-Q detector bank LA35 at 7 K and 95 K for MgReO₄ (a) and 140 K for ZnReO₄ (b). The monoclinic wolframite structures of (c) ZnReO₄ and (d) MgReO₄ illustrate the oxygen octahedra surrounding Re atoms in the *a-b* plane and *a-c* plane.

one third is expected to be parallel to it (causing an exponentially decaying tail). We verify the asymmetry ratios between the tail and AFM oscillations in Appendix C.

As the temperature increases above T_N , the oscillations evolve to a static Gaussian Kubo-Toyabe (KT) multiplied by an exponential type depolarization [45], describing muon spin relaxation in a system of randomly oriented static spins within the muon lifetime. We use LF measurements to confirm KT to be the most suitable polarization function (Appendix D). Furthermore, the spins are already decoupled at a small applied magnetic field of 20 Gauss, indicating that the spin distribution above T_N arises from nuclear moments, which appear static within the muon lifetime. To account for all these processes within the considered temperature range, the ZF data for both samples was fitted with the following polarization function:

$$\begin{aligned}
 A_0 P_{ZF}(t) = & A_{AF1} \cos\left(2\pi f_{AF1} + \frac{\pi\phi}{180}\right) e^{-\lambda_{AF1}t} \\
 & + A_{AF2} \cos\left(2\pi f_{AF2} + \frac{\pi\phi}{180}\right) e^{-\lambda_{AF2}t} \\
 & + A_{KT} G^{SGKT}(t, \Delta_{KT}) e^{-\lambda_{KT}t} \\
 & + A_{tail} e^{-\lambda_{tail}t} \\
 & + A_{Im} e^{-\lambda_{Im}t},
 \end{aligned} \tag{1}$$

where $P_{ZF}(t)$ is the muon polarization in ZF, A_i the corresponding asymmetry, λ_i the

damping, ν_i and ϕ_i the frequency and phase of the oscillations, and Δ_{KT} the Gaussian distribution width of the KT and λ_{KT} the relaxation rate of the KT. In addition to the AF1, AF2 and KT contributions, the polarization has two exponentially decaying terms; a very slowly decaying tail, λ_{tail} coming from the magnetic moments parallel to the initial muon spin polarization, and a decaying signal λ_{Im} attributed to impurities in the sample. A similar impurity phase has been found in both compounds and it has previously been speculated for MgReO_4 to arise from Re impurities [36]. In the fitting, the impurity fraction A_{Im} is fixed to a value determined from TF measurements at low temperature (see Appendix E). Furthermore, the phase of AF oscillations is theoretically $\phi = 0$. However, uncertainty in the muon implantation time, wide internal field distributions, and incommensurate (IC) order can cause $\phi \neq 0$, and therefore, it was treated as a fitted parameter. We confirm, however, that the fitted value remains close to zero at base temperature, and the phase is constrained to be the same for the two muon sites, AF1 and AF2.

3.2.1 MgReO_4

The raw data for the MgReO_4 μ^+ SR analysis is the same as in Ref. [36]. In this work, we reanalyze it with a greater focus on determining a detailed spin structure and comparing it with ZnReO_4 . The ZF muon spectra and temperature dependence of the polarization function (Eq. (1)) fitting parameters of MgReO_4 are shown in Fig. 2. Above T_N , A_{KT} dominates, as expected for a paramagnetic sample. As the temperature is lowered, this asymmetry decreases in favor of A_{AF1} , A_{AF2} and A_{tail} indicative of a magnetic ordering with the transition temperature $T_N = 83.35(2)$ K with the error being a statistical error in the fit (Appendix E).

The two oscillations AF1 and AF2 suggest the existence of two different muon stopping sites in the AFM temperature regime. Looking further into the fitting coefficients we can note that AF2 has a substantially larger asymmetry than AF1 ($A_{\text{AF2}} \approx 10A_{\text{AF1}}$). Since asymmetry reflects the fraction of muons experiencing a given local field, the larger asymmetry for AF2 suggests that the majority of muons stopping in the sample do so at the AF2 muon site. Furthermore, the relaxation rate λ_{AF2} is larger than λ_{AF1} , indicating a broader field distribution at the site. However, λ_{AF1} has significantly larger error bars, likely due to fitting difficulties from the small volume fraction.

In MgReO_4 the AF1 frequency is no longer distinguishable at around $T \geq 60$ K. To ensure that the muon site population is truly suppressed rather than simply becoming indistinguishable from the other site as the frequencies decrease, we attempted to fix the ratio between the two frequencies of AF1 and AF2. However, with this, the frequency AF1 is still no longer resolvable at $T = 60$ K. This suggests that that one muon stopping site is no longer populated in the range $60 \text{ K} < T < T_N$.

At $T \approx 50$ K we see indications of a small, but sharp jump in asymmetry A_{AF1} , coinciding with a lower precession frequency. While this could be indicative of a second magnetic transition, we suggest that it is more likely an artifact of the fitting, as disregarding the 50 K point, the frequency evolution seems to follow the power law trend. Furthermore, if there was a magnetic transitions occurring at this temperature, we would expect it to be visible in magnetic susceptibility, which we do not observe [36].

Moreover, as the frequency AF1 disappears, we see a gradual increase in asymmetry for AF2. Our analysis suggests that the disappearance of the AF1 muon site at 60 K is better explained by changes in the muon site population rather than spin canting, as previously hypothesized in [36](Sec. 3.3).

Finally, we have reanalyzed the critical exponent β of MgReO_4 by fitting the frequency

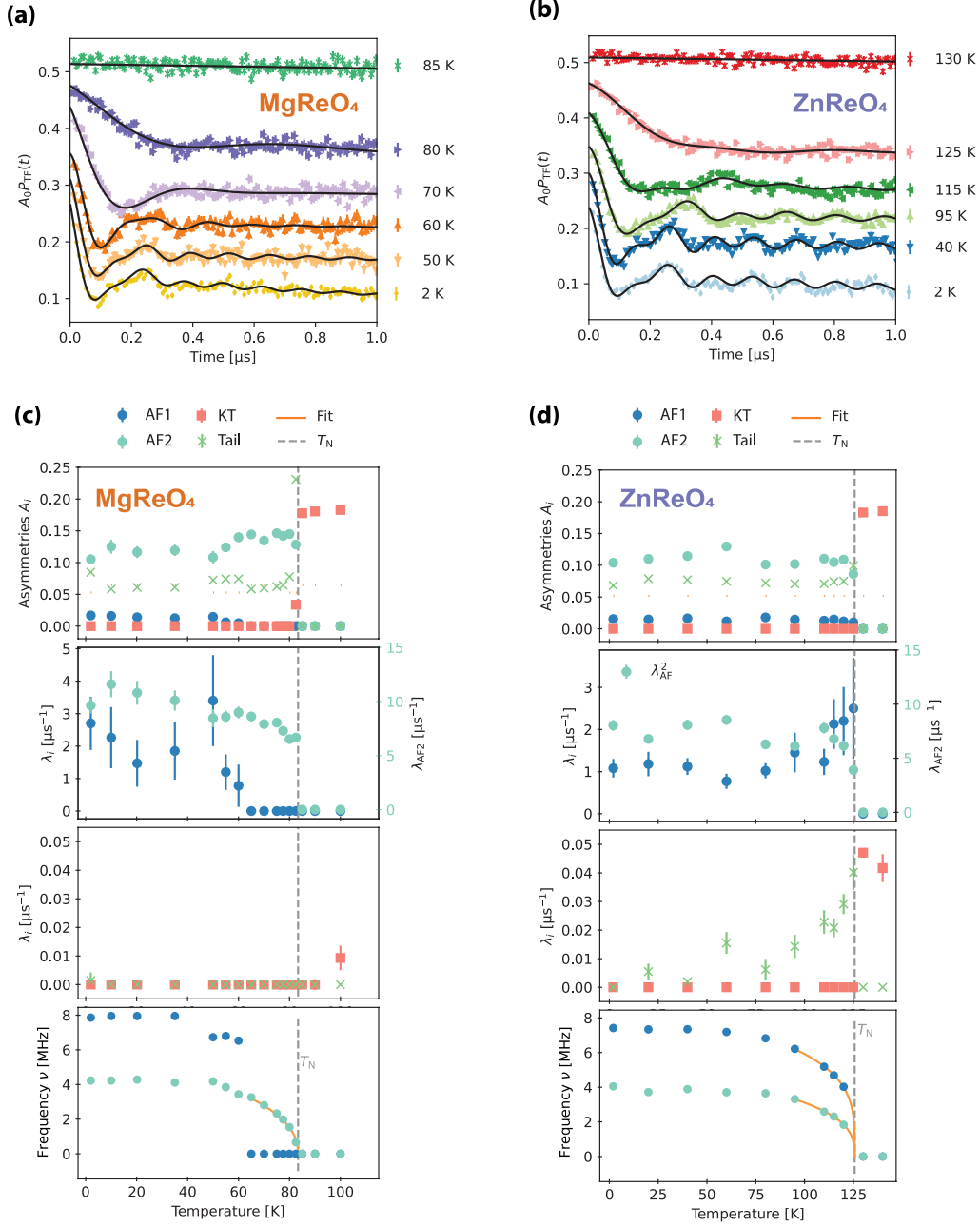


Figure 2: Muon spin spectroscopy (μ^+ SR) zero field (ZF) data and corresponding fit lines in black using polarization function (eq. (1)) for (a) MgReO₄ and (b) ZnReO₄. Temperature dependent ZF coefficients from polarization function (eq. (1)) for (c) MgReO₄ and (d) ZnReO₄. The Néel temperatures, $T_N^{\text{Mg}} = 83.35(2)$ K $T_N^{\text{Zn}} = 126.67(10)$ K, are marked with a gray line. The oscillation frequencies are fitted with a power law near transition temperature with $\beta_1^{\text{Zn}} = 0.35(1)$, $\beta_2^{\text{Zn}} = 0.26(1)$ and $\beta_1^{\text{Mg}} = 0.41(1)$.

to the mean-field power law:

$$f = \alpha \left(1 - \frac{T}{T_N}\right)^\beta, \quad (2)$$

using only temperature points near the transition (from 65 K to a fixed $T_N = 83.35(2)$ K). This fitting yields a critical exponent of $\beta^{\text{Mg}} = 0.41$, though variations in T_N within its error margins introduces a $\pm 10\%$ uncertainty, with the choice of temperature range for the fitting contributing an even larger error. The critical exponents is not inconsistent with a three dimensional order parameter [46]. However, the large error due to lack of measurements close to the transition makes it difficult to draw any definitive conclusions about the universality class of the transition.

3.2.2 ZnReO₄

As in MgReO₄, A_{KT} dominates above T_N [Fig. 2 d)], and with lowered temperature this asymmetry decreases in favor of A_{tail} , A_{AF1} and A_{AF2} , indicative of a magnetic ordering. However, ZnReO₄ exhibits a significantly higher $T_N = 125.67(10)$ K (Appendix E). Similar to MgReO₄, it is notable that AF2 has a substantially larger asymmetry ($A_{\text{AF2}} \approx 7A_{\text{AF1}}$), again indicating the favoring of muon site AF1. The asymmetry, as an indicator of muon site population, is subsequently used to evaluate the possible magnetic structures of the compounds (Sec. 3.3). Additionally, the relaxation rate λ_{AF2} is higher than λ_{AF1} by a factor of two, similar to MgReO₄.

We can see that λ_{AF1} , as well as λ_{tail} reaches a cusp at T_N , as expected near a phase transition. In this case λ_{tail} is larger and can therefore be fitted more accurately than for MgReO₄. In ZnReO₄ both frequencies are present throughout the entire AFM phase, indicating that the loss of one observed muon precession frequency is specific to MgReO₄.

Finally, the critical exponents for ZnReO₄, obtained by fitting the frequency from 95 K to a fixed $T_N = 126.67$ K using Eq.(2), are $\beta_1^{\text{Zn}} = 0.35(1)$ and $\beta_2^{\text{Zn}} = 0.26(1)$ also consistent with a three dimensional order parameter, as in MgReO₄. As with MgReO₄, the critical exponents have large errors due to the uncertainty in T_N and the choice of temperature range. The temperature range used is a compromise between the number of data points and staying close to the transition.

3.3 Muon site and field calculations

To resolve the magnetic structure and the origin behind the disappearing frequency in MgReO₄, we conducted self consistent calculations using Quantum ESPRESSO [40] to determine the electrostatic potentials in the compounds. Here, we did not consider local distortions due to the implanted muon, as the two compounds do not contain mobile ions and their structures are already quite distorted. Therefore, any small perturbation from the muon is unlikely to have a significant effect. Our calculations suggest two potential muon sites [Tab. 2], which are only slightly shifted along the b axis between the compounds.

First, to confirm the muon site calculations, we calculate the spherical average of the internal field distribution width arising from the nuclear moments, Δ as

$$\Delta_{\text{ZF}}^2 = 2 \left(\frac{\mu_0}{4\pi} \right)^2 \sum_i \frac{\gamma_i^2 \hbar^2 I_i(I_i + 1)}{r_i^6} \frac{1}{3}, \quad (3)$$

where r_i is the distance of the i^{th} nucleus, and γ_i and I_i are the gyromagnetic ratio and nuclear spin of the nucleus [47]. The calculated values [Tab. 2] fit the experimental values quite well.

With the muon sites confirmed, we calculated local magnetic fields for various spin structures based on our previous approaches [48–50]. We assume the local field is primarily dipolar, as hyperfine coupling effects have been shown to be minimal, even in an A-type AFM [48]. To calculate the possible magnetic structures, we use irreducible representation

(IR) analysis, a powerful symmetry-based method that places strict limits on the allowed moment directions for a given crystal structure [51].

From the literature on other magnetic wolframite compounds, FeWO₄ is reported to adopt an AFM structure with $\mathbf{k} = (1/2, 0, 0)$ and moments along a , while under hydrostatic pressure, the spins become canted in the ac -plane [52]. Similarly, NiWO₄ [53] and MnWO₄ [54] exhibit canted AFM spin structures in the ac -plane. In these compounds, the magnetic ions occupy the $2f$ Wyckoff site, while Re in our compounds is at the $2e$ site. This difference swaps the allowed moment directions for each IR: those permitting moments in the ac -plane for the $2f$ site correspond to moments only allowed along b in our case, and vice versa.

Based on the related wolframite compounds, we calculated the local magnetic field for $\mathbf{k} = (0, 0, 0)$, $\mathbf{k} = (0, 1/2, 0)$ and $\mathbf{k} = (1/2, 0, 0)$. When calculating the different spin configurations, we accounted for the probability distribution of the muon sites and used that the size of the measured asymmetry is proportional to the muon stopping probability. The three \mathbf{k} -vectors, $\mathbf{k} = (0, 0, 0)$, $(0, 1/2, 0)$, $(1/2, 0, 0)$ share the same 4 IRs [Table 3], two of which allow the spins only along the b -axis, while the other two allow spins to point in the ac -plane, but depending on the \mathbf{k} -vector they result in different magnetic structures. For $\mathbf{k} = (0, 0, 0)$, Γ_1 and Γ_3 are FM structures, while Γ_2 and Γ_4 are AFM. For $\mathbf{k} = (0, 1/2, 0)$ and $(0, 0, 1/2)$, all structures are AFM, with Γ_4 yielding the same structure as for $\mathbf{k} = (0, 0, 0)$.

For completeness, the local field based on a magnetic structure with $\mathbf{k} = (0, 0, 1/2)$ was also calculated. This wave vector has only one IR, which, when canted, forms a non-collinear structure. This structure is tunable through internal degrees of freedom and can also result in a collinear configuration with spins along b . However, this structure was not consistent with the measured frequencies in ZF μ^+ SR.

The other \mathbf{k} -vectors revealed three possible spin structures which we found could reproduce the measured μ^+ SR frequencies. One structure, Γ_3 with $\mathbf{k} = (1/2, 0, 0)$ has a magnetic moment of $\mu = 0.77\mu_B$, because the muon sites are positioned between two AFM coupled spins. As a result, a larger magnetic moment is needed to induce the same muon precession frequencies. This structure was disregarded, as such a large moment would be detectable with NPD. The remaining two structures, which both involve spin canting away from the principal axes in the ac -plane and exhibit low magnetic moments, closely match the experimental data [Tab. 2]. The difference between the structures is that in Γ_3 with $\mathbf{k} = (0, 1/2, 0)$, the Re atoms that are further separated along b are FM coupled, while in Γ_4 with $\mathbf{k} = (0, 0, 0)$, they are AFM coupled [Fig. 3].

To explore the possibility of a reduction in the number of precession frequencies due to spin canting in MgReO₄, we allow the spins to rotate in the ac -plane, which is the only distortion direction allowed for the Γ_3 and Γ_4 IRs. Our calculations show that the two muon sites can begin to experience the same internal magnetic field at specific canting angles for Γ_4 . However, this would mean that the lower frequency AF2 would rise to 6 MHz, which we do not observe. Otherwise, the frequency ratio could be consistent with canting if both magnetic sites experienced a sudden drop in the magnitude of the moment, which we would not expect at a spin canting transitions when there is no accompanying structural transition (see Appendix F). Therefore, it is unlikely that spin canting is responsible for the disappearing frequency.

3.4 Bond Valence Sum

The magnetic structure and moment size of MgReO₄ and ZnReO₄ are very similar. Interestingly, Re⁶⁺ has been previously reported to have an effective moment of $\mu = 1.2 - 1.7\mu_B$, while Re⁵⁺ and Re⁷⁺ have been reported to have much weaker effective moment of

MgReO₄			
Muon site	f_{AFM} (MHz)	Δ_{MgReO_4} (μs^{-1})	Δ_{KT} (μs^{-1})
$\mu_1(0.0, 0.37, 0.75)$	4.229(9)	0.135	0.232(11)
$\mu_2(0.5, 0.12, 0.25)$	7.86(7)	0.156	0.232(11)

Γ_3		
$k = (0, \frac{1}{2}, 0)$	$\mu = 0.295\mu_{\text{B}}$	Canting angle 51°
Muon site	$B_{\text{dip}'}$ (G)	$f_{\text{dip}'}$ (MHz)
μ_1	[0.01306, 0, -0.02835]	4.23
μ_2	[0.04902, 0, -0.03136]	7.89

Γ_4		
$k = (0, 0, 0)$	$\mu = 0.255\mu_{\text{B}}$	Canting angle 37.5°
Muon site	$B_{\text{dip}'}$ (G)	$f_{\text{dip}'}$ (MHz)
μ_1	[-0.05291, 0, 0.02301]	4.185
μ_2	[0.00097, 0, -0.03086]	7.82

ZnReO₄			
Muon site	f_{AFM} (MHz)	Δ_{ZnReO_4} (μs^{-1})	Δ_{KT} (μs^{-1})
$\mu_1(0.0, 0.39, 0.75)$	4.05(5)	0.136	0.1207(4)
$\mu_2(0.5, 0.14, 0.25)$	7.42(3)	0.158	0.1207(4)

Γ_3		
$k = (0, \frac{1}{2}, 0)$	$\mu = 0.292\mu_{\text{B}}$	Canting angle 56°
Muon site	$\mathbf{B}_{\text{dip}'}$ (G)	$f_{\text{dip}'}$ (MHz)
μ_1	[-0.01209, 0, 0.02725]	4.04
μ_2	[0.04397, 0, -0.03278]	7.43

Γ_4		
$k = (0, 0, 0)$	$\mu = 0.242\mu_{\text{B}}$	Canting angle 39.5°
Muon site	$\mathbf{B}_{\text{dip}'}$ (G)	$f_{\text{dip}'}$ (MHz)
μ_1	[-0.00027, 0, 0.02994]	4.06
μ_2	[0.04981, 0, -0.02268]	7.42

Table 2: The obtained muon sites and experimental data for MgReO₄ and ZnReO₄ are presented, along with calculated dipolar fields for two proposed magnetic structures, Γ_3 and Γ_4 . The table includes the internal field distribution of nuclear moments (Δ_{KT}), experimentally obtained frequencies (f_{AFM} from ZF fit), and field distributions (Δ_{MgReO_4} and Δ_{ZnReO_4} from fitting). Also shown are the magnetic structures, wave vector k , moment μ , and canting angle (relative to the a -axis). Muon precession frequencies are calculated as $f_{\text{dip}'} = (\gamma_{\mu}/2\pi)|\mathbf{B}_{\text{dip}'}|$, where $\mathbf{B}_{\text{dip}'}$ is the dipolar magnetic field at the muon site and γ_{μ} is the muon gyromagnetic ratio.

$\mu = 0.3 - 0.8\mu_{\text{B}}$ [20]. Considering the expected value of the oxidation of Re^{6+} being much higher than our estimation, as well as not visible in NPD, it may be appropriate to assign different oxidation states for Re in MgReO₄ and ZnReO₄. We therefore employ bond

Table 3: Irreducible representations (IRs) of the little group for propagation vectors $\mathbf{k} = (0, 0, 0), (0, 1/2, 0), (1/2, 0, 0)$ in space group $P2/c$. The symmetry operators are given in Seitz notation and the IRs are calculated using BasIreps. The allowed moment directions are indicated for each IR.

IR	$\{1 000\}$	$\{2_{0y0} 00p\}$	$\{-1 000\}$	$\{m_{x0z} 00p\}$	Moment
Γ_1	1	1	1	1	(0,v,0)
Γ_2	1	1	-1	-1	(0,v,0)
Γ_3	1	-1	1	-1	(u,0,w)
Γ_4	1	-1	-1	1	(u,0,w)

valence sum (BVS) analysis which uses the bond lengths to nearby atoms to estimate the oxidation state of the atom. BVS analysis assumes an perfect correlation between bond length and oxidation state, which may be influenced by local structural distortions. Further validation through complementary techniques, such as X-ray absorption spectroscopy (XAS), could strengthen these findings.

The bond length between atoms is directly correlated with the oxidation state, generally resulting in a higher oxidation state when the bond length is shorter. The bond length is however also dependent on the atom size, which is not a well defined quantity, and depends on the charge carrier density around the atom. There are multiple ways to calculate the relation between bond length and bond flux and one of the most simple and still very robust methods is BVS. For more details of the method see Ref. [56].

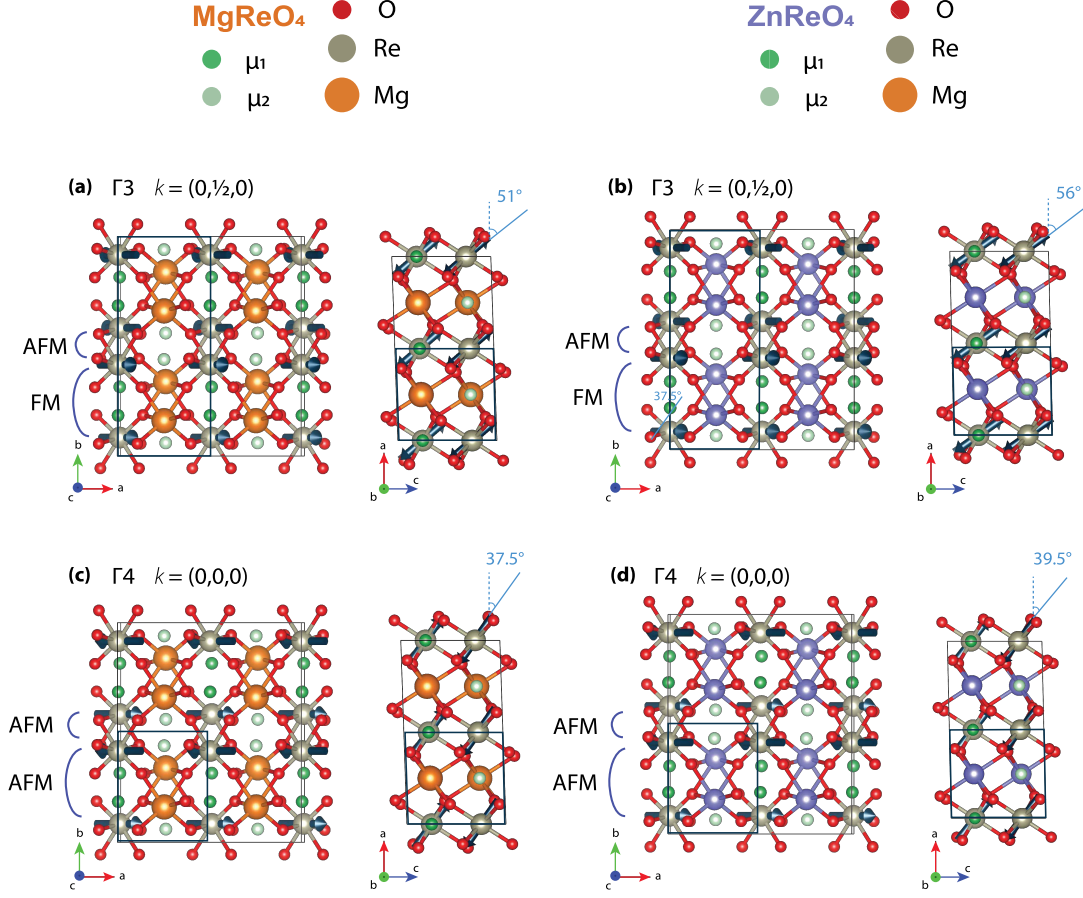


Figure 3: Proposed magnetic structures for irreducible representations (IRs) Γ_3 and Γ_4 , drawn with VESTA [55]. (a, b) Γ_3 for MgReO_4 and ZnReO_4 , respectively. (c, d) Γ_4 for MgReO_4 and ZnReO_4 . The unit cell is doubled along a and b , with the magnetic unit cell outlined in blue. Muon sites (green) and spin structures (dark arrows) are shown. In both cases, the moments lie in the ac -plane, canting away from the a -axis by different amounts corresponding to the values which reproduce the experimental frequencies found in μ^+ SR.

In BVS, the valence V is defined as as

$$V = \sum_i s_i = \sum_i e^{(R_0 - R_i)/b}, \quad (4)$$

where R_0 is the reference bond length corresponding to valence +1, specific to each cation-anion pair, R_i is the distance between atom i and the center atom and s_i is the experimentally obtained bond valence. The parameter b controls how rapidly the bond valence decreases or increases with a change in bond length. For most oxides, b is empirically found to be approximately 0.37 \AA [57].

Since our system involves typical ionic or covalent bonds, the standard value of $b = 0.37 \text{ \AA}$ is appropriate. Since R_0 varies between each kind of pair of atoms it needs to first be empirically determined from a set of well characterized compounds. However, the empirically determined R_0 can only be applied for atoms having a similar range of bond lengths. An extensive list of bond valences has been summarized by Brown [58]. Unfortunately,

no value for R_0 is reported for Re^{6+} . However, for Re^{7+} , a value of $R_0^{\text{Re}^{7+}} = 1.943 \text{ \AA}$ is given [59], and unconfirmed reports for other oxidation states suggest values around $R_0 \approx 1.9 \text{ \AA}$ [58]. Given the similar atomic sizes, it is likely that R_0 for Re^{6+} does not differ significantly from this value.

To find the value of $R_0^{\text{Re}^{6+}}$, we have looked at other Re^{6+} compounds (MnReO_4 [35] and $\text{Sr}_3\text{Re}_2\text{O}_9$ [26]) BVS. We begin by calculating the BVS for Mn and Sr in the reference materials, both of which are close to the expected value of 2 [Tab. 4]. Then, we determine R_0 for Re^{6+} by fitting it using a least-squares approach and known crystal structures. The obtained R_0 values are very similar, ranging from 1.91 to 1.92. Since this is close to the reported R_0 value for Re^{7+} , it gives us confidence that the BVS values should be reliable for our materials.

Compound	Bond	V	R_0 [\AA]
MnReO_4	Mn - O	1.948	1.740 [60]
$\text{Sr}_3\text{Re}_2\text{O}_9$	Sr - O	2.084	1.765 [61]
Fitted	MnReO_4	$\text{Sr}_3\text{Re}_2\text{O}_9$	
R_0^{6+}	1.9111(7)	1.9206(5)	

Table 4: Bond valence sums (BVS) for Mn-O in MnReO_4 (structure [35]) and Sr-O in $\text{Sr}_3\text{Re}_2\text{O}_9$ (structure [26]), along with the fitted R_0 values for Re-O for these compounds.

MgReO_4	Bond	V	R_0 [\AA]
	Mg - O	1.981	1.693 [62]
	Re - O	6.091	1.9111(7)
ZnReO_4	Bond	V	R_0 [\AA]
	Zn - O	1.903	1.704 [62]
	Re - O	6.55	1.9111(7)

Table 5: Calculated bond valence sums (BVS) for MgReO_4 and ZnReO_4 , using $R_0 = 1.91$ from MnReO_4 for Re - O (Tab. 4).

We can now use this to investigate the BVS in MgReO_4 and ZnReO_4 (Tab. 5). To apply the BVS analysis, the bond lengths of the reference sample must be comparable. We chose the R_0 value for Re^{6+} from MnReO_4 , as it exhibits the most similar bond length variation to our samples (1.80 \AA - 2.05 \AA). The bond length ranges in our samples are 1.79 \AA to 2.08 \AA for MgReO_4 and 1.74 \AA to 2.10 \AA for ZnReO_4 .

Unfortunately, the bond length range for ZnReO_4 is more than 0.1 \AA larger than that for the reference sample MnReO_4 , making it difficult to reliably calculate the BVS for ZnReO_4 . This larger variance may stem from Zn having a full 3d electron shell, which leads to stronger ligand interactions and increased flexibility in bond lengths. Additionally, Zn^{2+} is susceptible to second-order JT distortions, causing asymmetries in the ligand arrangement [63]. In contrast, MgReO_4 does not experience these effects as strongly because Mg^{2+} lacks d-electrons, resulting in weaker ligand-metal interactions and a more symmetric structure.

For MgReO_4 our calculations results in BVS, $V_{\text{Re-O}} = 6.115$ and $V_{\text{Mg-O}} = 1.981$, suggesting Re^{6+} . Since MgReO_4 and ZnReO_4 exhibit similar magnetic behavior as seen from $\mu^+\text{SR}$, we can reasonably assume the Re to be in the same oxidation state Re^{6+} for

ZnReO₄ as well.

4 Discussion

Both compounds have a wolframite-type nuclear structure with distorted octahedral coordination of O around the Re atoms. It is in fact not uncommon for Re⁷⁺, Re⁶⁺ and Re⁵⁺ to stabilize in distorted octahedron configuration with O [20, 64]. In other compounds, distortions of the octahedral center has been shown to be due to Re - Re bonds within the oxide, causing varying distances between the Re atoms [33, 65]. In our study, the observed Re-Re distances are relatively long - about 4.5 Å for both MgReO₄ and ZnReO₄ - compared to the bond length in ReO₂, which is 2.48 Å [33], making Re-Re bonds unlikely to be responsible for the distortions.

A possible cause of the distorted octahedra is JT distortions, which occur in octahedral complexes with degeneracy in the *d*-orbitals [66]. To break the degeneracy, the structure undergoes distortion, lowering the crystal symmetry. This type of distortion is plausible for 5*d*¹ electron systems, such as Re⁶⁺, and could therefore cause the distorted octahedral configuration in our compounds. Second-order JT distortions from Zn²⁺ could account for the more distorted structure found in ZnReO₄.

The ZF polarization function coefficients of the two compounds hold many similarities [Fig. 2]. At low temperatures, both compounds display two oscillations, AF1 and AF2, with similar frequencies (about 4 MHz and 8 MHz), indicating the presence of two muon stopping sites. The relaxation rates, λ_i , are also similar. A difference between the compounds is that for ZnReO₄, λ_{tail} reaches a cusp at T_N , as expected with the onset of fluctuations at a phase transition. This kind of cusp is however not visible for MgReO₄, which could be due to the even smaller asymmetry of AF1 in MgReO₄ or fitting difficulties due to the impurity fraction.

The main distinction between the compounds is the number of frequencies reduces to one in MgReO₄ for $T \geq 60$ K, which we previously speculated to be due to spin canting [36]. Here, we suggest that spin canting is unlikely to be the cause of the missing frequency. Instead, we note that the volume fraction of AF1 is very small, and uncertainty in λ_{AF1} high. It is therefore possible that small perturbations, such as thermal expansion of the unit cell or changes in the octahedral distortion, could alter the electric field distribution in such a way that the muon site is no longer populated. A temperature dependent structural study, combined with corresponding DFT calculations of the electronic structure could resolve this scenario.

The two suggested magnetic structures [Fig. 3] have low magnetic moments ($0.29(5)\mu_B$ for Γ_3 and $0.25(8)\mu_B$ for Γ_4), much lower than what is expected for Re^{6+} ($1.2 - 1.7 \mu_B$). The low moment is further confirmed by lack of a magnetic contribution detectable in the NPD patterns. BVS calculations confirm MgReO_4 to be in the Re^{6+} oxidation state, with likely a similar result for ZnReO_4 . This raises the question of why the magnetic moment is so low in both MgReO_4 and ZnReO_4 , which μ^+ SR data shows is of similar magnitude.

In fact other Re^{6+} oxides have been found exhibiting moments as low as $0.3 - 0.8 \mu_B$ [43, 67, 68]. This suppression is attributed to SOC being strong enough to cause a splitting in the t_{2g} orbitals into a lower energy $J_{\text{eff}} = 3/2$ quartet and higher energy $J_{\text{eff}} = 1/2$ doublet [69]. The quartet has a theoretical effective magnetic moment of zero, but a non-zero moment is typically observed. In a DFT study addressing $5d^1$ electron systems, such as Re^{6+} , this effect has been attributed to hybridization between the d orbital with the ligand p orbitals [70]. In the same study, they also show that distortion to the octahedral configuration also causes an increase in magnetic moment, but that this quite quickly saturates as it distorts from an ideal octahedra, aligning with the fact that we see similar magnetic moment in both compounds, even when ZnReO_4 has a more distorted octahedral configuration.

We investigated two compounds with remarkably similar magnetic properties at base temperature, despite Zn and Mg having different electronic configurations. This suggests that spin-orbit coupling (SOC) is responsible for the suppressed moment, consistent with similar effects observed in other Re^{6+} oxides. Bramnik *et al.* [35] also observed a lower-than-expected paramagnetic moment in MnReO_4 , considering a different oxidation state scenario ($\text{Mn}^{2+}/\text{Re}^{7+}$), but ruled this out based on bond lengths. Their analysis similarly supports that the compound remains in the Re^{6+} . This indicates that the suppressed magnetic moment is a characteristic feature of Re^{6+} compounds with octahedral oxygen coordination, largely independent of the other metals in the material.

Further, studying the temperature dependence of the lattice parameters, specifically across T_N , would deepen our understanding of the relationship between octahedral distortion and magnetic moment in these Re^{6+} oxides.

5 Conclusions

Using NPD we have been able to characterize the monoclinic wolframite structure of ZnReO_4 and MgReO_4 , completing the structure description first reported by Sleight *et al.* [23]. Both compounds show distorted octahedral coordination of O around the Re, with larger distortion in ZnReO_4 .

Using μ^+ SR and ACMS, we have found MgReO_4 and ZnReO_4 to be AFM with respective $T_N = 83.35(2)$ and $T_N = 125.67(10)$. Furthermore, in the AFM phase, we find two muon sites with a similar temperature dependence in ZnReO_4 , in contrast to MgReO_4 , where the number of frequencies reduces to one at $T \geq 60$ K. Our results are most consistent with one muon site becoming suppressed (less populated) with higher temperature, which could be caused by a temperature-induced change in the electronic structure that significantly decreases the muon stopping probability for that site. High-resolution structural measurements and DFT calculations would help clarify this.

Muon site calculations reveal two possible AFM structures, with the spins canted away from the a -axis in the ac -plane: Γ_3 with $\mathbf{k} = (0, 1/2, 0)$ and Γ_4 with $\mathbf{k} = (0, 0, 0)$, for both MgReO_4 and ZnReO_4 . The ordered moments of $0.29(5)\mu_B$ for Γ_3 and $0.25(8)\mu_B$ for Γ_4 are consistent with the lack of magnetic contribution seen in the NPD patterns below T_N . In this case, the muon, being a highly sensitive magnetic probe, is one of the only ways of

getting insight into the subtle magnetic properties of these materials.

The obtained ordered magnetic moment is significantly smaller than the expected moment for mononuclear Re^{6+} compounds (1.2 - 1.7 μ_{B}). Our bond valence sum (BVS) analysis shows that the Re^{6+} state applies for MgReO_4 and most likely also applies for ZnReO_4 . Therefore, we propose that SOC together with d - p ligand hybridization is the cause of the suppressed observed ordered moment.

We investigated two compounds with similar magnetic properties, despite different electronic configurations in Zn and Mg. Our results suggest that SOC suppresses the magnetic moment, a feature consistent with other Re^{6+} oxides. This suppressed moment appears to be characteristic of Re^{6+} compounds with octahedral oxygen coordination, regardless of the other metals present in the compound.

Acknowledgements

We would like to thank A. Kentaro Inge from Stockholm University for his assistance with the XRD. NPD beamtime was performed at J-PARC using the iMATERIA instrument (Proposal Number: 2024A0387), and we are grateful for the technical assistance provided by the local staff. μ^+ SR measurements were conducted at the General Purpose Surface Muon (GPS) instrument at PSI (Experimental number: 20221283). We sincerely appreciate the invaluable support and expertise of the facility staff.

Funding information The research is funded by the Swedish Research Council, VR (Dnr. 2021-06157 and Dnr. 2022-03936), the Swedish Foundation for Strategic Research (SSF) within the Swedish national graduate school in neutron scattering (SwedNess), the Carl Tryggers Foundation for Scientific Research (CTS-22:2374), and the Knut and Alice Wallenberg Foundation through the grant 2021.0150. U.M. acknowledges funding from the KTH-SCI doctoral excellence program. J.S. was supported by the Japan Society for the Promotion of Science (JSPS) KAKENHI Grant No. JP23H01840 and JP24H00042. O.K.F. is supported by the Swedish Research Council (VR) via a Grant 2022-06217 and the Foundation Blanceflor 2023 and 2024 fellow scholarships. E.N. acknowledges financial support from the SSF-Swedness grant SNP21-0004 and the Foundation Blanceflor 2024 fellow scholarship.

Data Availability and Analysis: The data and analysis supporting this study are available from the corresponding authors upon reasonable request.

A AC Magnetic Susceptibility

The real part of the AC magnetic susceptibility (ACMS) signal as a function of temperature can be found in Fig. 4. From the measurement, we can identify $T_{\text{N}} \approx 126$ K. The sharp increase below $T = 100$ K is likely due to ferromagnetic (FM) impurity, similar as seen in transportation measurements for MgReO_4 [36] and which can be identified as a paramagnetic background in the muon spin spectroscopy (μ^+ SR) data. As the cusp is very small, we see that the magnetic signal is quite weak. Due to the impurities, it is difficult to fit the ACMS data to extract the magnetic moment. We should also note that some more sample degradation may have occurred in the sample mounting process as the capsule was exposed to air during transport.

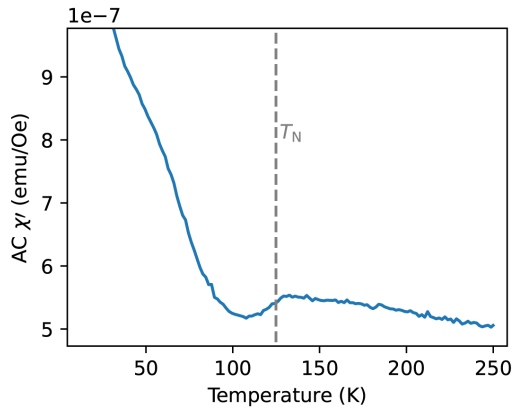


Figure 4: Real part of AC Magnetic Susceptibility signal of ZnReO_4 as a function of temperature. Grey line indicates $T_N = 125.67 \text{ K}$ obtained from $\mu^+\text{SR}$

B XRD analysis

In an attempt to determine the crystal structure and the atomic positions in MgReO_4 and ZnReO_4 , XRD patterns were collected at room temperature. The patterns were collected using the Single Crystal X-ray Diffractometer Bruker D8 VENTURE (1:2 ratio of $\text{CuK}\alpha_1$ and $\text{CuK}\alpha_2$ radiation, Göbel mirror, transmission mode, step size 0.02°). Because of the high X-ray absorption of rhenium, the sample was mounted on a glass fiber coated in Dow Corning high vacuum grease. The glass fiber was then mounted in a quartz capillary (diameter 0.3 mm) and sealed in an argon environment. The diffraction spectra were refined using FULLPROF SUITE [38]. We collected approximately double the statistics in the XRD pattern for MgReO_4 than ZnReO_4 .

After refinement of the neutron powder diffraction (NPD) data, it was understood that the samples must have begun degrading by reacting with the hydrogen present in the grease in the mounting procedure. The refined structures are highly distorted, especially for ZnReO_4 . Following is the description of the refinement from the XRD measurements.

The measured peaks [Fig. 5 a)-b)] could best be identified using a monoclinic wolframite structure with the space group $\text{P}2/c$ (# 13) [44]. The refined lattice parameters [Tab. 6] are close to the values found by Sleigh *et al.* [23]. The structure [Fig. 5 c)-d)] contains edge-sharing distorted octahedral coordination of O surrounding the Re atoms. The octahedra form a zig-zag formation along the c -axis and sandwiches the Mg/Zn atoms along the a -axis [Fig. 5 c)-d)]. In the distorted octahedra of MgReO_4 , the Re-O-Re bond angles range from 73° to 111° , while in ZnReO_4 , they vary from 62° to 136° , both significantly deviating from the ideal 90° . Additionally, the octahedra are compressed along the a -axis and elongated along the c -axis. The Re center is also displaced along the b -axis, leading to varying Re-Re distances along this direction.

Both samples exhibit large impurity peaks around $2\theta = 25^\circ - 30^\circ$. The impurities could not be refined to any known compound containing O, Re and/or Mg/Zn and the regions containing these peaks were therefore excluded in the refinement.

Parameter	ZnReO ₄
Crystal structure	monoclinic P2/c
a, b, c (Å)	4.69510, 5.60900, 5.02330
β (°)	91.2600
V (Å ³)	132.2557
Zn (x, y, z)	(0.5, 0.67400, 0.25)
Re (x, y, z)	(0, 0.16850, 0.25)
O1 (x, y, z)	(0.17100, 0.10500, 1.02600)
O2 (x, y, z)	(-0.05500, 0.66100, 0.42700)
Refinement	
χ^2	24.49
Excluded region (°)	0 - 14, 25.3 - 30.0

Parameter	MgReO ₄
Crystal structure	monoclinic P2/c
a, b, c (Å)	4.68210, 5.57500, 5.00710
β (°)	92.0260
V (Å ³)	130.619952
Mg (x, y, z)	(0.5, 0.0.67600, 0.25)
Re (x, y, z)	(0, 0.16330, 0.25)
O1 (x, y, z)	(0.11900, 0.16200, 0.91200)
O2 (x, y, z)	(-0.19800, 0.60500, 0.60200)
Refinement	
χ^2	12.16
Excluded region (°)	0 - 14, 25.5 - 28.0

Table 6: Crystal structure parameters of ZnReO₄ and MgReO₄ from refinement of powder XRD data.

C Zero Field

We can verify the origin of the tail component in the zero field (ZF) polarization function by checking that the sum of AFM asymmetries ($\frac{2}{3}$ of the signal) divided by two corresponds to the tail signal. Fig. 6 shows that these quantities align well in our case below T_N for ZnReO₄, implying that the tail component indeed arises due to spins parallel to the initial muon spin polarization.

D Longitudinal Field

Longitudinal field (LF) measurements were conducted in order to confirm a suitable ZF polarization function to be used above T_N . The moments are decoupled already at 20 G in both MgReO₄ and ZnReO₄, indicating static nuclear spin distribution above T_N . The most suitable polarization function is therefore KT described by the following polarization function

$$A_0 P_{KT}(t) = A_{KT} G^{SGKT}(t, \Delta_{KT}) e^{-\lambda_{KT} t} \quad (5)$$

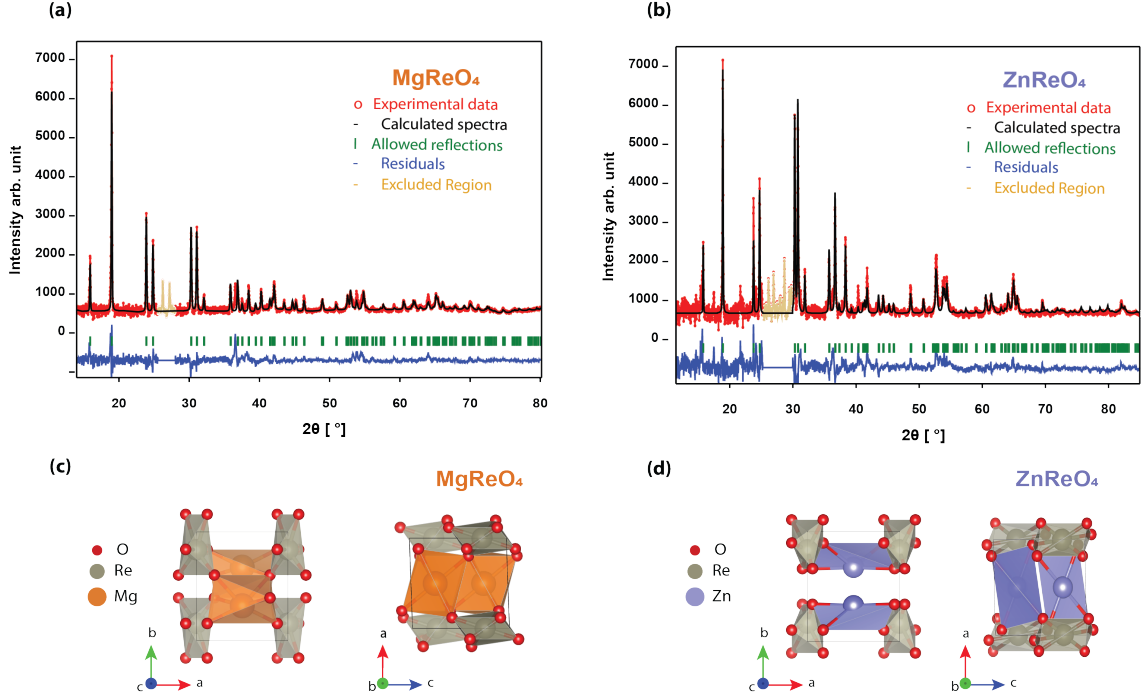


Figure 5: Powder X-ray diffraction pattern for (a) ZnReO_4 and (b) MgReO_4 respectively, showing the measured pattern, fitted spectra, allowed reflections and residuals. Excluded regions, due to impurities are removed in the plot. Monoclinic wolframite structure of (c) ZnReO_4 and (d) MgReO_4 , showing the highly distorted oxygen octahedra formed around Re atoms in the $a - b$ plane and $a - c$ plane due to sample degradation.

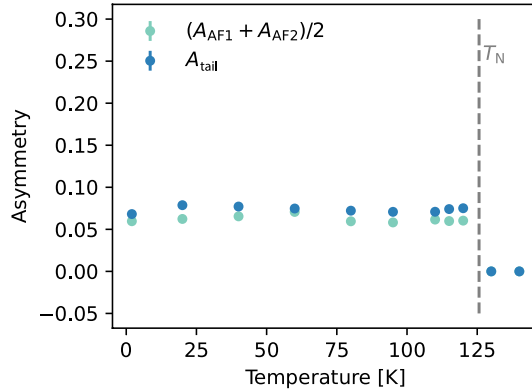


Figure 6: The sum of asymmetries of the two AF oscillatory terms from polarization function (eq. (1)) in ZnReO_4 divided by two plotted together with the tail asymmetry.

where A_{KT} is the KT asymmetry, λ_{KT} is the exponential damping, and Δ_{KT} the Gaussian distribution width of the KT. Appendix Fig. 7 shows the measured spectra and fitted polarization function above T_N for MgReO_4 and ZnReO_4 for an applied LF of 0 G, 10 G and 20 G. Here, the total asymmetry and field distribution Δ_{KT} is common for all applied fields.

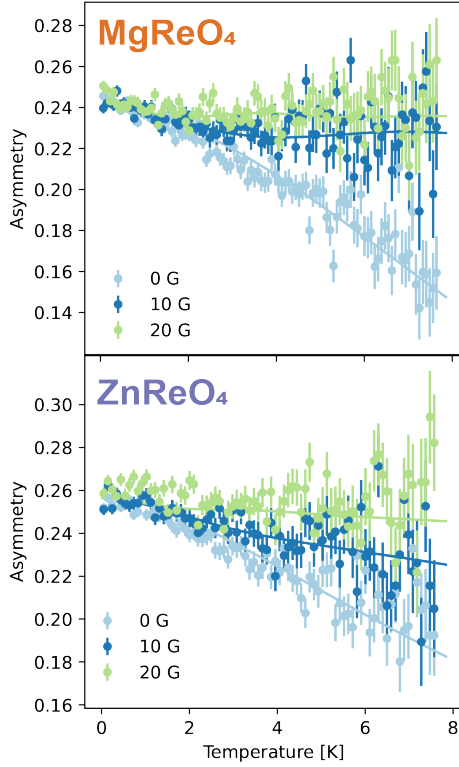


Figure 7: Longitudinal field (LF) measurements and fitted Kubo-Toyabe (KT) polarization function of MgReO_4 and ZnReO_4 for applied fields of 0 G, 10 G and 20 G at temperatures of 100 K and 140 K respectively.

E Transverse Field

μ^+ SR measurements in applied transverse field (TF) of $B = 50$ G for both MgReO_4 and ZnReO_4 (selected temperatures for ZnReO_4 visible in Fig. The data [Fig. 8]) is best described by the polarization function:

$$\begin{aligned}
 A_0 P_{\text{TF}}(t) = & A_{\text{TF}} \cos\left(2\pi f_{\text{TF}} + \frac{\pi\phi_{\text{TF}}}{180}\right) e^{-\lambda_{\text{TF}}t} \\
 & + A_{\text{AF}} \cos\left(2\pi f_{\text{AF}} + \frac{\pi\phi_{\text{AF}}}{180}\right) e^{-\lambda_{\text{AF}}t} \\
 & + A_{\text{tail}} e^{-\lambda_{\text{tail}}t},
 \end{aligned} \tag{6}$$

where $P_{\text{TF}}(t)$ is the muon polarization in TF and A_0 the total asymmetry, which for our experimental setup is $A_0 \approx 0.25$. The polarization function is made up of three contributions; two relaxed oscillating terms coming from the applied TF and inner AFM field, and a slowly decaying magnetic tail arising from the internal magnetic moments which are parallel to the muon spin. In the polarization function, A_i denotes the corresponding asymmetry, λ_i the damping, and f_i and ϕ_i the frequency and phase of the oscillations. In theory, we have $\phi = 0$, but uncertainties in implantation times, broad internal field distributions, and IC orders can cause $\phi \neq 0$, so the parameter was fitted. However, we confirm that the value is close to 0 at the base temperature.

Fitting the temperature dependence of the TF coefficients [Fig. 9] with a sigmoid function, allows us to extract T_N for ZnReO_4 as $T_N^{\text{Zn}} = 125.67(10)$ and $T_N^{\text{Mg}} = 83.35(2)$ for MgReO_4 , where the error represents the variance in temperature from the fitting results.

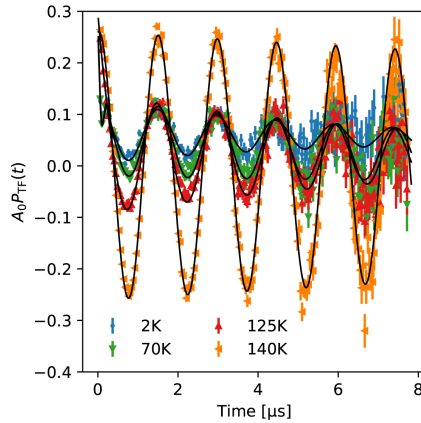


Figure 8: μ^+ SR data of MgReO_4 in transverse field (TF) of $B = 50 \text{ G}$ with errorbars and corresponding fits using polarization function (6) in black.

The TF asymmetry is not completely suppressed below T_N and stays $\approx 20\%$ for both compounds until base temperature. This is likely due to impurities in the samples.

Furthermore, we observe a peak in λ_{AF} before T_N for ZnReO_4 . We expect the relaxation rate to increase close to a phase transition with the onset of spin fluctuations associated. Therefore, we expect a cusp at the transition temperature. The reason we do not observe this for MgReO_4 could be due to the small AF1 asymmetry fraction.

We also see changes in the asymmetry distribution between the tail and AF component close to T_N for ZnReO_4 . This indicates that the two components become more difficult to distinguish closer to T_N and could be the cause of the relaxation rate dip before transition.

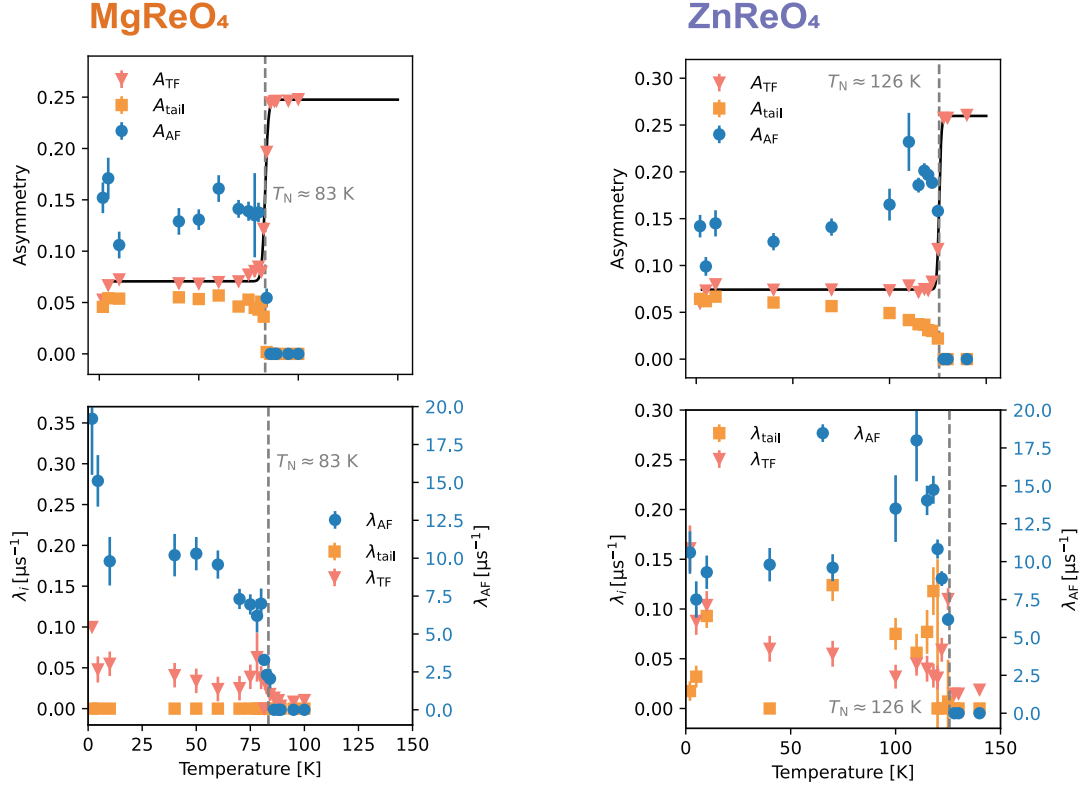


Figure 9: Temperature dependent TF coefficients from polarization function (6) for MgReO_4 (left) and ZnReO_4 (right). The Néel temperature $T_N^{\text{Zn}} = 125.67(10)$ K and $T_N^{\text{Mg}} = 83.35(2)$ K are marked in with a grey line. The TF asymmetry is fitted with a sigma function shown in black.

F Canting in MgReO_4

To examine the possibility of the canting scenario in MgReO_4 we let the spins cant within the ac plane using the IRs Γ_3 and Γ_4 . Fig. 10 shows the evolution of the two muon site frequencies as a function of canting angle. We see that for Γ_3 the two frequencies never fully meet and are always separated by at least 0.4 MHz. For Γ_4 , the two frequencies meet for the first time at 61° at 6.1 MHz. In our experiments we see that the higher frequency AF2 is no longer distinguishable, but we do not see a drastic increase in the lower frequency, which would be expected if the cause of the reduction in frequencies would be spin canting. Otherwise it would mean a sudden drastic decrease in the magnetic moment exactly coinciding with the lower frequency not changing noticeably. This seems quite unlikely, especially since we do not observe any structural transition in the compound in this temperature range either.

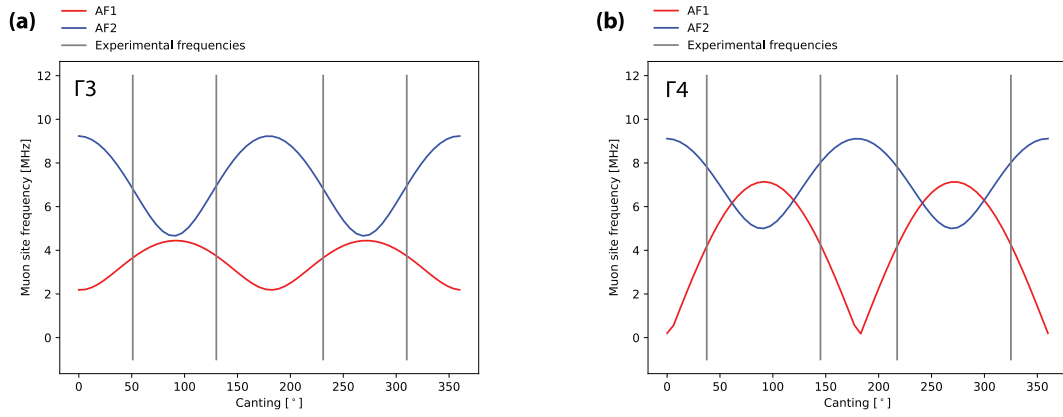


Figure 10: Experienced muon precession frequency and experimentally observed frequency from zero field muon spin spectroscopy μ^+ SR data for the two sites of MgReO_4 for the magnetic structures a) Γ_3 with $\mathbf{k} = (0, 1/2, 0)$ and b) Γ_3 with $\mathbf{k} = (0, 0, 0)$. Showing the muon sites experiencing the same frequency at a set of angles at around 6 MHz for Γ_4 , but not for Γ_3

References

- [1] W. E. Pickett, *Electronic structure of the high-temperature oxide superconductors*, Rev. Mod. Phys. **61**, 433 (1989), doi:10.1103/RevModPhys.61.433.
- [2] M. Shi, A. Bendounan, E. Razzoli, S. Rosenkranz, M. R. Norman, J. C. Campuzano, J. Chang, M. Månsson, Y. Sassa, T. Claesson, O. Tjernberg, L. Patthey *et al.*, *Spectroscopic evidence for preformed cooper pairs in the pseudogap phase of cuprates*, EPL **88**(2), 27008 (2009), doi:10.1209/0295-5075/88/27008.
- [3] M. Kargarian, A. Langari and G. A. Fiete, *Unusual magnetic phases in the strong interaction limit of two-dimensional topological band insulators in transition metal oxides*, Physical Review B **86**(20) (2012), doi:10.1103/physrevb.86.205124.
- [4] S.-H. Lee, Y. Qiu, C. Broholm, Y. Ueda and J. J. Rush, *Spin Fluctuations in a Magnetically Frustrated Metal LiV_2O_4* , Physical Review Letters **86**(24), 5554–5557 (2001), doi:10.1103/physrevlett.86.5554.
- [5] Q. Faure, S. Takayoshi, V. Simonet, B. Grenier, M. Månsson, J. S. White, G. S. Tucker, C. Rüegg, P. Lejay, T. Giamarchi and S. Petit, *Tomonaga-Luttinger liquid spin dynamics in the quasi-one-dimensional Ising-like antiferromagnet $BaCo_2V_2O_8$* , Phys. Rev. Lett. **123**(2), 027204 (2019), doi:10.1103/PhysRevLett.123.027204.
- [6] C. Jia, S. Onoda, N. Nagaosa and J. H. Han, *Microscopic theory of spin-polarization coupling in multiferroic transition metal oxides*, Phys. Rev. B **76**(14), 144424 (2007), doi:/10.1103/PhysRevB.76.144424.
- [7] M. Soda, S. Hayashida, B. Roessli, M. Månsson, J. S. White, M. Matsumoto, R. Shiina and T. Masuda, *Continuous control of local magnetic moment by applied electric field in multiferroics $Ba_2CoGe_2O_7$* , Phys. Rev. B **94**(9) (2016), doi:10.1103/PhysRevB.94.094418.
- [8] V. Heine and L. F. Mattheiss, *Metal-insulator transition in transition metal oxides*, J. Phys. C: Solid State Phys. **4**(10), L191 (1971), doi:10.1088/0022-3719/4/10/003.
- [9] M. Imada, A. Fujimori and Y. Tokura, *Metal-insulator transitions*, Rev. Mod. Phys. **70**(4), 1039 (1998), doi:10.1103/revmodphys.70.1039.
- [10] C. Yuan, H. B. Wu, Y. Xie and X. W. D. Lou, *Mixed transition-metal oxides: Design, synthesis, and energy-related applications*, Angewandte Chemie International Edition **53**(6), 1488 (2014), doi:/10.1002/anie.201303971.
- [11] H. Su, S. Jaffer and H. Yu, *Transition metal oxides for sodium-ion batteries*, Energy Storage Materials **5**, 116 (2016), doi:/10.1016/j.ensm.2016.06.005.
- [12] P. Benedek, O. K. Forsslund, E. Nocerino, N. Yazdani, N. Matsubara, Y. Sassa, F. Jurányi, M. Medarde, M. Telling, M. Månsson and V. Wood, *Quantifying diffusion through interfaces of lithium-ion battery active materials*, ACS Appl. Mater. Interfaces **12**(14), 16243 (2020), doi:10.1021/acsami.9b22792.
- [13] S. Dey, G. C. Dhal, D. Mohan and R. Prasad, *Advances in transition metal oxide catalysts for carbon monoxide oxidation: A review*, Adv. Compos. Hybrid Mater. **2**(4), 626 (2019), doi:10.1007/s42114-019-00126-3.

- [14] A. Yusuf, C. Snape, J. He, H. Xu, C. Liu, M. Zhao, G. Z. Chen, B. Tang, C. Wang, J. Wang and S. N. Behera, *Advances on transition metal oxides catalysts for formaldehyde oxidation: A review*, *Catalysis Reviews* **59**(3), 189–233 (2017), doi:10.1080/01614940.2017.1342476.
- [15] C. N. R. Rao, *Transition metal oxides*, *Annu. Rev. Phys. Chem.* **40**(1), 291 (1989), doi:10.1146/annurev.pc.40.100189.001451.
- [16] W. Noddack, I. Tacke and O. Berg, *Die ekamangane*, *Naturwissenschaften* **13**(26), 567 (1925), doi://doi.org/10.1007/BF01558746.
- [17] W. A. Herrmann, *High oxidation state organometallic chemistry: A challenge—the example of rhenium*, *Angew. Chem. Int. Ed.* **27**(10), 1297 (1988), doi:10.1002/anie.198812971.
- [18] C. Chay, M. Avdeev, H. E. A. Brand, S. Injac, T. A. Whittle and B. J. Kennedy, *Crystal structures and phase transition behaviour in the 5d transition metal oxides $AReO_4$ ($A = Ag, Na, K, Rb, Cs, \text{ and } Tl$)*, *J. Chem. Soc., Dalton Trans.* **48**(47), 17524 (2019), doi:10.1039/c9dt04021h.
- [19] D. Mikhailova, H. Ehrenberg and H. Fuess, *Synthesis and structure determination of copper perrhenate, $CuReO_4$* , *J. Solid State Chem.* **179**(7), 2004 (2006), doi:10.1016/j.jssc.2006.03.039.
- [20] G. Rouschias, *Recent advances in the chemistry of rhenium*, *Chem. Rev.* **74**(5), 531 (1974), doi:10.1021/cr60291a002.
- [21] A. M. Affoune, J. Bouteillon and J. C. Poinet, *Electrochemical behaviour of perrhenate ions in molten alkali fluorides*, *J. Appl. Electrochem.* **25**(9), 886 (1995), doi:10.1007/bf00772210.
- [22] N. Zhumasheva, L. Kudreeva, A. Kalyeva and G. Badavamova, *Electrodeposition process of perrhenate ions from kno_3 and na_2so_4 background electrolytes in the presence of citric acid*, *Chem. Bull. Kazakh Natl. Univ.* **96**(1)(1), 4 (2020), doi:10.15328/cb1087.
- [23] A. Sleight, *New Ternary Oxides of Pentavalent and Hexavalent Rhenium of the Type $AReO_4$ or A_2ReO_6* , *Inorg. Chem.* **14**, 597 (1975), doi:10.1021/ic50145a032.
- [24] W. H. Baur, W. Joswig, G. Pieper and D. Kassner, *$CoReO_4$, a new rutile-type derivative with ordering of two cations*, *J. Solid State Chem.* **99**(1), 207–211 (1992), doi:10.1016/0022-4596(92)90307-h.
- [25] C. E. Frank, E. E. McCabe, F. Orlandi, P. Manuel, X. Tan, Z. Deng, M. Croft, V. Cascos, T. Emge, H. L. Feng, S. Lapidus, C. Jin *et al.*, *Mn_2CoReO_6 : a robust multisublattice antiferromagnetic perovskite with small A-site cations*, *Chem. Commun.* **55**(23), 3331 (2019), doi:10.1039/c9cc00038k.
- [26] D. Urushihara, T. Asaka, K. Fukuda, M. Nakayama, Y. Nakahira, C. Moriyoshi, Y. Kuroiwa, O. K. Forslund, N. Matsubara, M. Månsson, K. Papadopoulos, Y. Sassa *et al.*, *Structural Transition with a Sharp Change in the Electrical Resistivity and Spin–Orbit Mott Insulating State in a Rhenium Oxide, $Sr_3Re_2O_9$* , *Inorg. Chem.* **60**(2), 507 (2021), doi:10.1021/acs.inorgchem.0c02750.

- [27] C. A. Marjerrison, C. M. Thompson, G. Sala, D. D. Maharaj, E. Kermarrec, Y. Cai, A. M. Hallas, M. N. Wilson, T. J. S. Munsie, G. E. Granroth, R. Flacau, J. E. Greedan *et al.*, *Cubic Re^{6+} ($5d^1$) Double Perovskites, Ba_2MgReO_6 , Ba_2ZnReO_6 , and $Ba_2Y_{2/3}ReO_6$: Magnetism, Heat Capacity, μ SR, and Neutron Scattering Studies and Comparison with Theory*, *Inorg. Chem.* **55**(20), 10701 (2016), doi:10.1021/acs.inorgchem.6b01933.
- [28] K. G. Bramnik, H. Ehrenberg and H. Fuess, *Preparation, Crystal Structure, and Magnetic Studies of a New $Sr_7Re_4O_{19}$ Double Oxide and Its Relation to the Structure of $Ba_7Ir_6O_{19}$* , *J. Solid State Chem.* **160**(1), 45 (2001), doi:10.1006/jssc.2001.9182.
- [29] K. G. Bramnik, H. Ehrenberg, J. K. Dehn and H. Fuess, *Preparation, Crystal Structure, and Magnetic Properties of Double Perovskites M_2MgReO_6 ($M = Ca, Sr, Ba$)*, *Solid State Sci.* **5**(1), 235 (2003), doi:10.1016/s1293-2558(02)00097-3.
- [30] D. Hirai, T. Yajima, K. Nawa, M. Kawamura and Z. Hiroi, *Anisotropic Triangular Lattice Realized in Rhenium Oxychlorides $A_3ReO_5Cl_2$ ($A = Ba, Sr$)*, *Inorg. Chem.* **59**(14), 10025 (2020), doi:10.1021/acs.inorgchem.0c01187.
- [31] J. Jelonek, A. Chełkowski, W. Zarek, G. Chełkowski and A. Winiarska, *Magnetic Properties of $REAl_6Fe_6$ Compounds for $RE \equiv Y, Dy, \text{ and } Ho$* , *J. Less Common Met.* **160**(2), 273 (1990), doi:10.1016/0022-5088(90)90387-y.
- [32] R. G. Pearson, *Concerning jahn-teller effects*, *Proc. Natl. Acad. Sci.* **72**(6), 2104 (1975), doi:10.1073/pnas.72.6.2104.
- [33] A. Magnéli, S. Siitonen, B. Skrifvars, J. Schliack and L. Reio, *Studies on rhenium oxides*, *Acta Chem. Scand.* **11**, 28 (1957), doi:10.3891/acta.chem.scand.11-0028.
- [34] L. E. Orgel, *Ferroelectricity and the structure of transition-metal oxides*, *Discuss. Faraday Soc.* **26**, 138 (1958), doi:10.1039/df9582600138.
- [35] K. G. Bramnik, H. Ehrenberg, S. Buhre and H. Fuess, *Preparation, crystal structure and magnetic properties of the high-pressure phase $MnReO_4$ with a wolframite-type structure*, *Acta Crystallogr. Sec. B Struc. Sc.* **61**(3), 246–249 (2005), doi:10.1107/s0108768105005380.
- [36] E. Nocerino, O. K. Forsslund, C. Wang, H. Sakurai, F. Elson, R. Palm, U. Miniotaita, Y. Ge, Y. Sassa, J. Sugiyama and M. Månsson, *Magnetic nature of wolframite $MgReO_4$* , *J. Phys.: Conf. Ser.* **2462**(1), 012037 (2023), doi:10.1088/1742-6596/2462/1/012037.
- [37] T. Ishigaki, A. Hoshikawa, M. Yonemura, T. Morishima, T. Kamiyama, R. Oishi, K. Aizawa, T. Sakuma, Y. Tomota, M. Arai, M. Hayashi, K. Ebata *et al.*, *Ibaraki materials design diffractometer (iMATERIA)–versatile neutron diffractometer at J-PARC*, *Nucl. Instrum. Methods Phys. Res. Sect. A* **600**(1), 189 (2009), doi:10.1016/j.nima.2008.11.137.
- [38] J. Rodríguez-Carvajal, *Recent advances in magnetic structure determination by neutron powder diffraction*, *Physica B Condens. Matter* **192**(1–2), 55 (1993), doi:10.1016/0921-4526(93)90108-i.
- [39] A. Suter and B. M. Wojek, *Musrfit: A free platform-independent framework for μ sr data analysis*, *Phys. Proc.* **30**, 69 (2012), doi:10.1016/j.phpro.2012.04.0422.

- [40] P. Giannozzi, S. Baroni, N. Bonini, M. Calandra, R. Car, C. Cavazzoni, D. Ceresoli, G. L. Chiarotti, M. Cococcioni, I. Dabo, A. Dal Corso, S. de Gironcoli *et al.*, *Quantum espresso: A modular and open-source software project for quantum simulations of materials*, J. Condens. Matter Phys. **21**(39), 395502 (2009), doi:10.1088/0953-8984/21/39/395502.
- [41] *muesr: A package for the calculation of muon stopping sites and related properties*, <https://muesr.readthedocs.io/>, Accessed: 2024-03-24 (2024).
- [42] M. Retuerto, M. J. Martínez-Lope, M. García-Hernández, M. T. Fernández-Díaz and J. A. Alonso, *Crystal and magnetic structure of Sr_2MReO_6 ($M = Ni, Co, Zn$) double perovskites: A neutron diffraction study*, Eur. J. Inorg. Chem. **2008**(4), 588 (2008), doi:10.1002/ejic.200700753.
- [43] S. Gao, D. Hirai, H. Sagayama, H. Ohsumi, Z. Hiroi and T.-h. Arima, *Antiferromagnetic Long-Range Order in the $5d^1$ Double-Perovskite Sr_2MgReO_6* , Phys. Rev. B **101**(22), 220412 (2020), doi:10.1103/physrevb.101.220412.
- [44] S. Dey, R. A. Ricciardo, H. L. Cuthbert and P. M. Woodward, *Metal-to-Metal Charge Transfer in AWO_4 ($A = Mg, Mn, Co, Ni, Cu, \text{ or } Zn$) Compounds with the Wolframite Structure*, Inorg. Chem. **53**(9), 4394 (2014), doi:10.1021/ic4031798.
- [45] R. S. Hayano, Y. J. Uemura, J. Imazato, N. Nishida, T. Yamazaki and R. Kubo, *Zero- and low-field spin relaxation studied by positive muons*, Physical Review B **20**(3), 850–859 (1979), doi:10.1103/physrevb.20.850.
- [46] G. Ódor, *Universality classes in nonequilibrium lattice systems*, Rev. Mod. Phys. **76**(3), 663 (2004), doi:10.1103/revmodphys.76.663.
- [47] A. Yaouanc and P. D. de Réotier, *Muon Spin Rotation, Relaxation, and Resonance*, International Series of Monographs on Physics. Oxford University Press, London, England (2010).
- [48] O. K. Forslund, H. Ohta, K. Kamazawa, S. L. Stubbs, O. Ofer, M. Månsson, C. Michioka, K. Yoshimura, B. Hitti, D. Arseneau, G. D. Morris, E. J. Ansaldo *et al.*, *Revisiting the A-type antiferromagnet $NaNiO_2$ with muon spin rotation measurements and density functional theory calculations*, Phys. Rev. B **102**(18), 184412 (2020), doi:10.1103/physrevb.102.184412.
- [49] O. K. Forslund, Y. Ge, H. Ohta, C. Wang, M. Abdel-Hafiez, J. Sugiyama, M. Månsson and Y. Sassa, *Refined Magnetic Structure of VI_3* , doi:10.48550/ARXIV.2210.17455 (2022).
- [50] O. K. Forslund, D. Andreica, H. Ohta, M. Imai, C. Michioka, K. Yoshimura, M. Månsson and J. Sugiyama, *Co-existence of Short- and Long-Range Magnetic Order in $LaCo_2P_2$* , Phys. Scr. **96**(12), 125864 (2021), doi:10.1088/1402-4896/ac3cf9.
- [51] E. Bertaut, *Representation analysis of magnetic structures*, Foundations of Crystallography **24**(1), 217 (1968).
- [52] O. Fabelo, J. Gonzalez-Platas, S. Savvin, P. Botella and D. Errandonea, *The Effect of Pressure on the Crystal and Magnetic Structure of $FeWO_4$* , J. Appl. Phys. **136**(17), 175901 (2024), doi:10.1063/5.0230576.

- [53] M. A. Prosnikov, V. Y. Davydov, A. N. Smirnov, M. P. Volkov, R. V. Pisarev, P. Becker and L. Bohatý, *Lattice and Spin Dynamics in a Low-Symmetry Antiferromagnet NiWO₄*, Phys. Rev. B **96**(1), 014428 (2017), doi:10.1103/physrevb.96.014428.
- [54] G. Lautenschläger, H. Weitzel, T. Vogt, R. Hock, A. Böhm, M. Bonnet and H. Fuess, *Magnetic Phase Transitions of MnWO₄ Studied by the Use of Neutron Diffraction*, Phys. Rev. B **48**(9), 6087–6098 (1993), doi:10.1103/physrevb.48.6087.
- [55] K. Momma and F. Izumi, *Vesta: A three-dimensional visualization system for electronic and structural analysis*, J. Appl. Crystallogr. **41**(3), 653 (2008), doi:10.1107/s0021889808012016.
- [56] I. D. Brown, *The Chemical Bond in Inorganic Chemistry: The Bond Valence Model*, vol. 12 of *International Union of Crystallography Monographs on Crystallography*, Oxford University Press, Oxford, ISBN 9780199298815 (2006).
- [57] I. D. Brown, *Recent developments in the methods and applications of the bond valence model*, Chem. Rev. **109**(12), 6858 (2009), doi:10.1021/cr900053k.
- [58] *Bond valence parameters—iucr.org*, <https://www.iucr.org/resources/data/datasets/bond-valence-parameters>, [Accessed 06-07-2024].
- [59] O. C. Gagné and F. C. Hawthorne, *Comprehensive derivation of bond-valence parameters for ion pairs involving oxygen*, Acta Crystallogr. B Struct. Sci. Cryst. Eng. Mater. **71**(5), 562 (2015), doi:10.1107/s2052520615016297.
- [60] O. C. Gagné and F. C. Hawthorne, *Comprehensive derivation of bond-valence parameters for ion pairs involving oxygen*, Acta Crystallographica Section B Structural Science, Crystal Engineering and Materials **71**(5), 562–578 (2015), doi:10.1107/s2052520615016297.
- [61] W. Liu and H. H. Thorp, *Bond valence sum analysis of metal-ligand bond lengths in metalloenzymes and model complexes. ii. refined distances and other enzymes*, Inorg. Chem. **32**(19), 4102 (1993), doi:10.1021/ic00071a023.
- [62] I. D. Brown and D. Altermatt, *Bond-valence parameters obtained from a systematic analysis of the inorganic crystal structure database*, Acta Crystallogr. B Struct. Sci. Cryst. Eng. Mater. **41**(4), 244 (1985), doi:10.1107/s0108768185002063.
- [63] W. Deng, Z. Li, Y. Ye, Z. Zhou, Y. Li, M. Zhang, X. Yuan, J. Hu, W. Zhao, Z. Huang, C. Li, H. Chen *et al.*, *Zn²⁺ Induced Phase Transformation of K₂MnFe(CN)₆ Boosts Highly Stable Zinc-Ion Storage*, Advanced Energy Materials **11**(31) (2021), doi:10.1002/aenm.202003639.
- [64] B. Krebs, A. Mueller and H. H. Beyer, *Crystal structure of rhenium (vii) oxide*, Inorg. Chem. **8**(3), 436 (1969), doi:/10.1021/ic50073a006.
- [65] M. T. K. Kolambage, G. Wetzels, K. Koehler, C. D. McMillen and J. W. Kolis, *Lanthanide Rhenium Oxide Single Crystals from Hydrothermal Fluids: Synthesis and Structures of Ln₂ReO₅ (Ln = Pr, Nd), Ln₃ReO₇ (Ln = Gd and Tb), and Ln₆ReO₁₂ (Ln = Yb, Lu)*, J. Solid State Chem. **306**, 122779 (2022), doi:10.1016/j.jssc.2021.122779.
- [66] H. A. Jahn and R. Teller, *The jahn-teller effect*, Proc. R. Soc. A **161**(905), 220 (1937), doi:10.1098/rspa.1937.0142.

- [67] D. Hirai, H. Sagayama, S. Gao, H. Ohsumi, G. Chen, T.-h. Arima and Z. Hiroi, *Detection of Multipolar Orders in the Spin-Orbit-Coupled 5d Mott Insulator Ba_2MgReO_6* , Phys. Rev. Res. **2**(2), 022063 (2020), doi:10.1103/physrevresearch.2.022063.
- [68] H. Ishikawa, D. Hirai, A. Ikeda, M. Gen, T. Yajima, A. Matsuo, Y. H. Matsuda, Z. Hiroi and K. Kindo, *Phase Transition in the $5d^1$ Double Perovskite Ba_2CaReO_6 Induced by High Magnetic Field*, Phys. Rev. B **104**(17), 174422 (2021), doi:/10.1103/PhysRevB.104.174422.
- [69] F. E. Mabbs and D. J. Machin, *Magnetism and Transition Metal Complexes*, Chapman and Hall, London, England (1973).
- [70] L. Xu, N. A. Bogdanov, A. Princep, P. Fulde, J. van den Brink and L. Hozoi, *Covallency and vibronic couplings make a nonmagnetic $j = 3/2$ ion magnetic*, npj Quantum Mater. **1**(1), 1 (2016), doi:10.1038/npjquantmats.2016.29.